Electrochemistry

DOI: 10.1002/anie.201001298

Fluorescent Cyclic Voltammetry of Immobilized Azurin: Direct Observation of Thermodynamic and Kinetic Heterogeneity**

Jante M. Salverda, Amol V. Patil, Giulia Mizzon, Sofya Kuznetsova, Gerhild Zauner, Namik Akkilic, Gerard W. Canters, Jason J. Davis, Hendrik A. Heering, and Thijs J. Aartsma**

The electrochemical analysis of surface-confined metalloproteins has resulted in a significant advance in our knowledge of the kinetic and thermodynamic nuances of biological electron transfer.[1] Surface confinement on a carefully engineered or appropriately modified electrode surface removes diffusion limitations in cyclic voltammetry, facilitates direct imaging or spectroscopic analyses, and requires small quantities of material. However, the associated voltammetric responses are typically nonideal, with broad voltammetric peaks and experiment-to-experiment variation.[2,3] Such observations have been loosely ascribed to kinetic and thermodynamic dispersion across the surface.[4–9] A range of causes may contribute to this variation, from lateral molecular interaction, variation in redox-site/electrode electronic coupling, to microenviromental variance in properties such as surface charge or molecular orientation.

This dispersion can be studied by taking advantage of the enhanced sensitivity of a newly developed method for monitoring redox-state transitions by fluorescence detection.[10–14] Herein, we have used azurin, a well-characterized 14 kDa large protein from *P. aeruginosa* with a single Cu ion as the redox-active center (see Figure S1 in the Supporting Information).[15–23] In its oxidized (Cu^{2+}) form, the protein displays a strong absorption at 630 nm, which is absent in the reduced state. This redox-dependent absorbance change can be monitored in the fluorescence domain by means of a Förster resonance energy transfer (FRET) donor–acceptor pair, whereby the redox site is the energy acceptor and an externally linked dye label is the fluorescent donor.

We applied fluorescence-detected cyclic voltammetry (FCV) to investigate both a full monolayer of protein (using epifluorescence detection) and a dilute sub-monolayer (using total internal reflection-excited fluorescence; TIRF). Figure 1 shows the conventional cyclic voltammogram and the simultaneously recorded FCV of Cy5-labeled wild-type (wt) azurin adsorbed on gold covered with a hexanethiol self-assembled monolayer (SAM), using epifluorescent detection, at a scan rate of 100 $mV\,s^{-1}$. Both signals have the shape expected for an immobilized protein at slow voltage scan rate (see sections 1–3 in the Supporting Information for details). A control analysis with Cy5-labeled redox-inactive Zn-azurin (section 4 in the Supporting Information) confirmed that the fluorescence switching of labeled Cu-azurin is due to the redox transition.

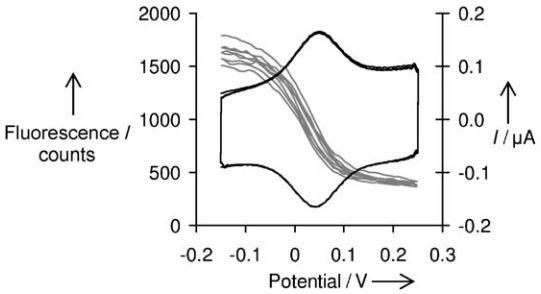

Figure 1. Cyclic voltammogram (black) and successive epifluorescent cyclic voltammograms (gray) of Cy5-labeled wt azurin at 100 $mV\,s^{-1}$ scan rate (4 cycles). The fluorescence change in FCV reflects the change in redox state of the labeled azurin.

FCVs measured at three different scan rates (Figure 2) show that the separation between oxidizing and reducing curves increases with scan rate, which is the same behavior as that for the peak separation in cyclic voltammetry (CV) experiments. The data points in these FCV curves were fitted by Butler–Volmer analysis (sections 5–7 in the Supporting Information, adapted from Heering et al.[24]).

[*] Dr. J. M. Salverda, N. Akkilic, Prof. Dr. T. J. Aartsma
Leiden Institute of Physics, Leiden University
PO Box 9504, 2300 RA Leiden (The Netherlands)
Fax: (+31) 71-527-5819
E-mail: aartsma@physics.leidenuniv.nl
Dr. A. V. Patil, G. Mizzon, Dr. J. J. Davis
Department of Chemistry, University of Oxford
Physical and Theoretical Chemistry Laboratory
South Parks Road, Oxford OX1 3QZ (UK)
Fax: (+44) 1865-275-410
E-mail: jason.davis@chem.ox.ac.uk
Dr. S. Kuznetsova, Dr. G. Zauner, Prof. Dr. G. W. Canters, Dr. H. A. Heering
Leiden Institute of Chemistry, Leiden University, Gorlaeus Laboratories
PO Box 9502, 2300 RA Leiden (The Netherlands)

[**] We are grateful to Laurent Holtzer for technical assistance, to Thyra de Jong, Lionel Ndamba, and Alessio Andreoni for protein purification, and to Ralf Schmauder, Leandro Tabares, Grzegorz Orlowski, and Razvan Stan for helpful discussions. J.M.S. and G.Z. were supported by the Foundation for Fundamental Research on Matter (FOM) and by a Veni grant (J.M.S.) from the Netherlands Organisation for Scientific Research (NWO). S.K. was funded by the program "From Molecule to Cell" from NWO. N.A. and G.M. were supported by the European Community through the EdRox Network (contract no. MRTN-CT-2006-035649). H.A.H. was funded by a Vidi grant from NWO. A.V.P. was funded by the Leverhulme Trust. The TIRF analyses described herein were carried out within the Nikon Oxford Molecular Imaging Centre (NOMIC).

Supporting information for this article is available on the WWW under http://dx.doi.org/10.1002/anie.201001298.

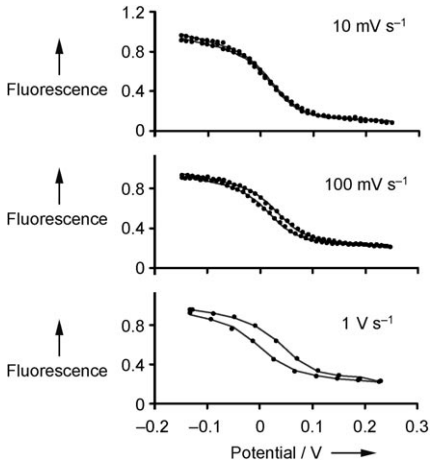

Figure 2. FCV curves measured at 10 mV s^{-1}, 100 mV s^{-1}, and 1 V s^{-1} showing scan-rate dependence.

From the scan-rate dependence of both CV and FCV, values for the midpoint potential E_0, electron-transfer rate constant k_0, and unusual quasi-reversibility UQR[25] were thus obtained (section 5 in the Supporting Information; Table 1).

Table 1: Fit parameters E_0, k_0, and UQR for CV and FCV.

Dataset	E_0 [mV][a]	k_0 [s^{-1}][b]	UQR[c]
CV	44	67	9.7 (1.0)
FCV	28	21	9.7 (fixed)

[a] Midpoint potential vs. SCE. [b] Standard electron-transfer rate constant. [c] Unusual quasi reversibility.

The kinetics of electron transfer determined by FCV are in reasonable agreement with those determined by CV.[21–23] The observed differences in k_0 values can be explained by the presence of heterogeneity in the electron-transfer rate. Owing to the bias of fluorescence detection towards proteins that are more weakly electronically coupled to the electrode (where fluorescence emission is less quenched), such heterogeneity results in a lower average rate in the optical sampling relative to the purely voltammetric results.

Heterogeneity is evident in the variance in fluorescence intensity across the surface (Figure 3a), which is typical for monolayer coverage. At low coverage, this variance is even more pronounced (section 2 in the Supporting Information). In Figure 3b, three FCV cycles of diffraction-limited spots (region-of-interest, or ROI, size $\approx$ 300 nm) show a large dispersion in the separation between the reducing and oxidizing curves, which is an observation diagnostic of a large dispersion in interfacial electron-transfer kinetics.

We quantified the kinetic and thermodynamic dispersion by constructing FCV cycles for over 200 such diffraction-limited ROIs at a range of scan rates. A ROI contains 500–3000 and 100–450 fluorescently labeled proteins for high-coverage and low-coverage samples, respectively (calculations in section 8 of the Supporting Information), which demonstrates an unprecedented molecular-scale electrochemical analysis. The results of fitting all ROI FCV cycles with Butler–Volmer curves are summarized in the histograms in Figure 4a–d (see also sections 5 and 6 in the Supporting Information).

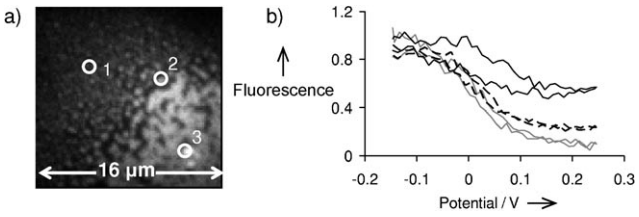

Figure 3. a) Image from the epifluorescence movie measured at 200 mV s^{-1} scan rate on wt azurin at monolayer coverage. b) Epifluorescent voltammograms for three ROIs of 1.5 pixel radius, selected from the image in (a): ROI 1 = gray line, ROI 2 = black dashed line, ROI 3 = black line.

The dispersions of E_0 and k_0 values are different for high and low protein coverage. In the former, we find a small spread in E_0 values (Figure 4a), which is dominated by noise (see section 9 in the Supporting Information), whereas significant dispersion is evident in the low-coverage data. The k_0 distributions show a high dispersion in both datasets (Figure 4c,d), but there is a qualitative difference between them. The low-coverage distribution is more asymmetric and contains a larger contribution from low electron-transfer rates (which is consistent with a data bias towards weakly coupled proteins).

The large k_0 dispersion at low coverage may be due to variation in the orientation of the protein with respect to the surface as well as to microscopic variation in the Au surface properties (local surface charges etc., that is, "microenvironmental variance"[5]). At these coverages, AFM and confocal analyses are consistent with significant molecular aggregation (data not shown). We propose that the analyzed kinetic distribution becomes biased towards faster k_0 values as surface coverage and film order increases (and there is a reduced weighting of the contribution from the aggregated forms, where k_0 is likely to be lower; Figure 4c,d).

As for E_0, at low coverage, the microenvironmental variance will strongly affect the midpoint potential and therefore the observed dispersion in E_0 values. At high molecular coverage, the effect of microenvironmental variance will be damped by sampling more molecules per ROI.

It is of interest to compare the present results with what is known from bulk measurements on electron transfer (ET) within protein–protein complexes and on ET between proteins and SAM-coated electrodes. As for the thermodynamics of the ET process, it is known that protein–protein or protein–electrode interactions can lead to significant modulation in the expressed half-wave potential within a range of 100 mV.[26–29] Haehnel and co-workers[29] have, for example, convincingly argued that the electric field exerted by a protein at the site of the redox-active cofactor of the partner protein may account for the observed variations in the midpoint potential.

Immobilization of a protein on a SAM-covered Au electrode may lead to changes of the same order of

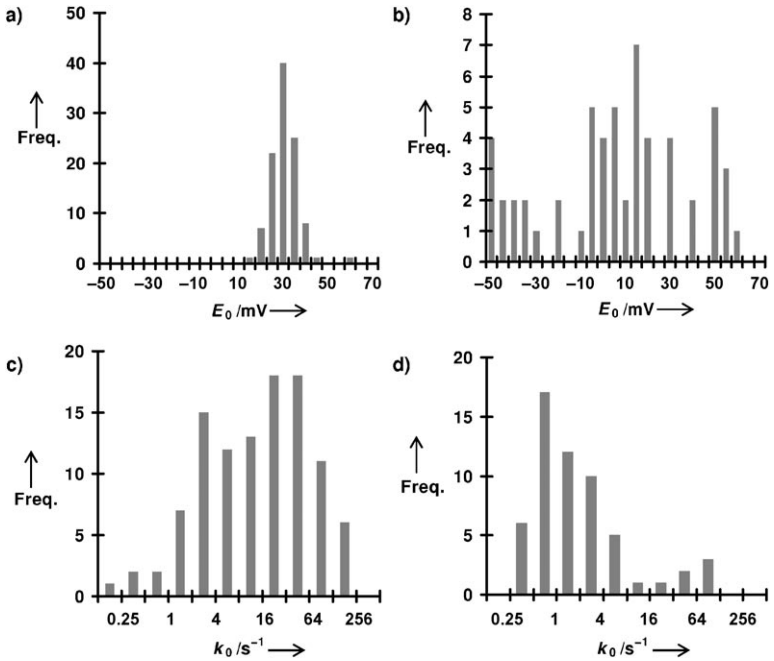

Figure 4. a) Histogram of midpoint potential values $E_0 = (E_{p,ox} + E_{p,red})/2$ obtained from all epifluorescence ROI FCV curves showing a 14 mV spread (FWHM) around an average of 28 mV. Bin values on the *x* axis refer to the upper limit of the bin range for all histograms shown. b) Histogram of midpoint potential values E_0 obtained from all TIRF ROI FCV curves showing a 70 mV spread (FWHM) around an average of 16 mV. c) Histogram of standard electron-transfer rate constants k_0 obtained from all epifluorescence ROI FCV curves showing values ranging from 0.1 s^{-1} to 200 s^{-1}. d) Histogram of standard electron-transfer rate constants k_0 obtained from all TIRF ROI FCV curves showing values clustering between 0.5 and 2 s^{-1} with a high-k_0 tail up to 100 s^{-1}.

magnitude. Murgida and Hildebrandt[30] have shown that the electric field at the boundary between solvent and SAM may be in the order of 10–100 mV Å^{-1} and may lead to similar changes in the midpoint potential of a redox protein that becomes immobilized on the SAM. In addition, the dielectric constant of the ET medium may be affected by the expulsion of water from the interface, and this may also influence the value of E_0.[29–31] The dispersion in the values of E_0 that we observe for the low-coverage data has a similar range (70 mV full width at half maximum; FWHM) as the mentioned values.[29,30] This result is ascribed to variations in the electric field that result from discontinuities or imperfections in the SAM or the underlying Au surface.

The kinetics of ET are strikingly similar between protein–protein and protein/Au–SAM data. It has been argued that ET within productive protein ET complexes occurs in the Marcus non-adiabatic limit and requires the formation of a specific complex.[32–34] The encounter complex between two proteins, however, may require mutual reorientation of the partners to reach the ET-competent configuration. Depending on the details of the protein surfaces and the protein–protein energy landscape,[35–37] this step may become rate-limiting.[30,32–34]

The rate of electron transfer between an ET protein and a SAM-coated Au electrode has been investigated as a function of the SAM thickness. At large distances, the non-adiabatic regime applies with an exponential $-(\beta R)$ distance dependence for the ET rate. At shorter distances, the rate becomes independent of SAM thickness,[21,23,38–41] either because the adiabatic limit now applies and the ET becomes friction controlled or because the protein has to reorient to reach an alignment with respect to the Au–SAM surface that is conducive for ET to or from the electrode.[30,42]

From studies on azurin and cytochrome *c* immobilized on a Au/hexanethiol SAM, the ET was found to be gated by protein reorientation.[23,43] In our experiments, we found that from one ROI to another there is appreciable variation in the value of k_0. This variation most likely reflects inhomogeneity of the tunneling barrier as a result of orientational flexibility. This must depend on parameters other than the electric field variation, which is responsible for the variation in E_0, since its value is averaged out at higher coverage. It is conceivable that differences in solvation and also in (local) coverage- and orientation-dependent lateral protein–protein interactions are critical in this respect.

In summary, we have demonstrated that the redox states of appropriately tagged surface-immobilized blue copper proteins can be optically sampled down to levels of a few hundred molecules, a sensitivity which is unprecedented for electrochemistry on a macroscopic surface. The thermodynamic midpoint potential was found to vary by tens of millivolts across the electrode surface, and the standard electron-transfer rate constant by more than a factor of 100. Furthermore, evidence for different types of heterogeneity was obtained by comparing high- and low-coverage data. To the best of our knowledge, the analysis herein constitutes the first direct observation of both kinetic and thermodynamic dispersion in a protein film on an electrode surface at a molecular scale of sampling.

Experimental Section

Sample preparation: Preparation and purification of wild-type and N42C azurin were carried out as previously described.[44] Wild-type (wt) azurin and zinc-reconstituted wt azurin were labeled on the N terminus as described by Kuznetsova et al.[12] The labeling ratio was 0.16. N42C azurin was prepared similarly (see section 10 in the Supporting Information). The labeling ratio for the N42C sample used was 0.55.

Sample immobilization and electrode preparation: The working electrode consisted of a semitransparent gold layer of 10 nm thickness deposited on a glass coverslip [1 inch (25.4 mm) diameter, thickness 0.14–0.17 mm (#1), Menzel]. Thin gold films were prepared either by RF sputtering (ATC 1800F, AJA International) or evaporation (Edward Auto 306 cryo evaporator). Sputtering was performed as described by van Baarle et al.[45] Azurin was immobilized on the working electrode through a self-assembling monolayer (SAM) of 1-hexanethiol (wt azurin) or 1-octanethiol (zinc azurin and N42C). For more details see section 11 in the Supporting Information.

Fluorescent electrochemistry setup: Measurements on wt azurin were performed with a wide-field epifluorescence microscopy setup (Zeiss Axiovert 200, Plan Apo 100X oil). A total internal reflection fluorescence (TIRF) setup (Nikon 2000-E, TIRF 100x Plan Apo oil) was used to perform FCV of immobilized N42C azurin at a surface coverage below the classical CV detection limit. Cy5 excitation was provided by a red diode laser (639 nm, Power Technology Inc., IQ1A30) for epifluorescence and by a HeNe laser (Model 1135, 20 mW, 633 nmn, JD Uniphase) for TIRF. Fluorescence was detected with a Peltier-cooled CCD camera (Cascade 512 X, Roper Scientific) or a back illuminated iCCD camera (iXon 885 EMCCD, Andor, Belfast, Northern Ireland), respectively. In both cases, fluorescence was measured in a series of images (a "movie") at fixed potential intervals (more details and a setup scheme in section 12 of the Supporting Information).

Electrochemistry: A copper wire connected the working electrode to a potentiostat (CH Instruments, model Chi832b, for epifluorescence, μ-Autolab, Eco Chemie, for TIRF). A Pt wire or Pt gauze counter electrode and saturated calomel (SCE) reference electrode (Radiometer Analytical/BASI) were inserted into a buffer droplet of approximately 100 μL on top of the immobilized protein film. CV scans were measured at rates of 10 $mV s^{-1}$ to 10 $V s^{-1}$, in potential steps of 1 mV. CV scanning was combined with epifluorescence detection up to 1 $V s^{-1}$ scan rate. TIRF FCV was measured at scan rates between 25 $mV s^{-1}$ and 600 $mV s^{-1}$.

Received: March 4, 2010
Revised: April 27, 2010
Published online: July 13, 2010

Keywords: cyclic voltammetry · electrochemistry · fluorescence · metalloproteins · monolayers

[1] P. Yeh, T. Kuwana, *Chem. Lett.* **1977**, 1145 – 1148.
[2] A. P. Brown, F. C. Anson, *Anal. Chem.* **1977**, *49*, 1589 – 1595.
[3] D. F. Smith, K. Willman, K. Kuo, R. W. Murray, *J. Electroanal. Chem.* **1979**, *95*, 217 – 227.
[4] G. K. Rowe, M. T. Carter, J. N. Richardson, R. W. Murray, *Langmuir* **1995**, *11*, 1797 – 1806.
[5] R. A. Clark, E. F. Bowden, *Langmuir* **1997**, *13*, 559 – 565.
[6] Z. Zhang, J. F. Rusling, *Biophys. Chem.* **1997**, *63*, 133 – 146.
[7] J. Hirst, F. A. Armstrong, *Anal. Chem.* **1998**, *70*, 5062 – 5071.
[8] L. J. C. Jeuken, F. A. Armstrong, *J. Phys. Chem. B* **2001**, *105*, 5271 – 5282.
[9] C. Léger, A. K. Jones, S. P. J. Albracht, F. A. Armstrong, *J. Phys. Chem. B* **2002**, *106*, 13058 – 13063.
[10] R. Schmauder, S. Alagaratnam, C. Chan, T. Schmidt, G. W. Canters, T. J. Aartsma, *J. Biol. Inorg. Chem.* **2005**, *10*, 683 – 687.
[11] R. Schmauder, F. Librizzi, G. W. Canters, T. Schmidt, T. J. Aartsma, *ChemPhysChem* **2005**, *6*, 1381 – 1386.
[12] S. Kuznetsova, G. Zauner, R. Schmauder, O. A. Mayboroda, A. M. Deelder, T. J. Aartsma, G. W. Canters, *Anal. Biochem.* **2006**, *350*, 52 – 60.
[13] J. J. Davis, H. Burgess, G. Zauner, S. Kuznetsova, J. Salverda, T. Aartsma, G. W. Canters, *J. Phys. Chem. B* **2006**, *110*, 20649 – 20654.
[14] S. Kuznetsova, G. Zauner, T. J. Aartsma, H. Engelkamp, N. Hatzakis, A. E. Rowan, R. J. M. Nolte, P. C. M. Christianen, G. W. Canters, *Proc. Natl. Acad. Sci. USA* **2008**, *105*, 3250 – 3255.
[15] C. M. Groeneveld, G. W. Canters, *J. Biol. Chem.* **1988**, *263*, 167 – 173.
[16] M. Van de Kamp, R. Floris, F. C. Hali, G. W. Canters, *J. Am. Chem. Soc.* **1990**, *112*, 907 – 908.
[17] H. Nar, A. Messerschmidt, R. Huber, M. Vandekamp, G. W. Canters, *J. Mol. Biol.* **1991**, *221*, 765 – 772.
[18] F. A. Armstrong, H. A. Heering, J. Hirst, *Chem. Soc. Rev.* **1997**, *26*, 169 – 179.
[19] U. Kolczak, C. Dennison, A. Messerschmidt, G. W. Canters in *Handbook of Metalloproteins* (Eds.: A. Messerschmidt, R. Huber, T. Poulos, K. Wieghardt), Wiley, Chichester **2001**, pp. 1170 – 1194.
[20] I. M. C. van Amsterdam, M. Ubbink, O. Einsle, A. Messerschmidt, A. Merli, D. Cavazzini, G. L. Rossi, G. W. Canters, *Nat. Struct. Biol.* **2002**, *9*, 48 – 52.
[21] J. J. Davis, D. Bruce, G. W. Canters, J. Crozier, H. A. O. Hill, *Chem. Commun.* **2003**, 576 – 577.
[22] J. Zhang, S. X. Guo, A. M. Bond, M. J. Honeychurch, K. B. Oldham, *J. Phys. Chem. B* **2005**, *109*, 8935 – 8947.
[23] Q. J. Chi, O. Farver, J. Ulstrup, *Proc. Natl. Acad. Sci. USA* **2005**, *102*, 16203 – 16208.
[24] H. A. Heering, M. S. Mondal, F. A. Armstrong, *Anal. Chem.* **1999**, *71*, 174 – 182.
[25] S. W. Feldberg, I. Rubinstein, *J. Electroanal. Chem.* **1988**, *240*, 1 – 15.
[26] J. M. Smith, W. H. Smith, D. B. Knaff, *Biochim. Biophys. Acta Bioenerg.* **1981**, *635*, 405 – 411.
[27] C. J. Batie, H. Kamin, *J. Biol. Chem.* **1981**, *256*, 7756 – 7763.
[28] K. A. Gray, V. L. Davidson, D. B. Knaff, *J. Biol. Chem.* **1988**, *263*, 13987 – 13990.
[29] F. Drepper, M. Hippler, W. Nitschke, W. Haehnel, *Biochemistry* **1996**, *35*, 1282 – 1295.
[30] D. H. Murgida, P. Hildebrandt, *Chem. Soc. Rev.* **2008**, *37*, 937 – 945.
[31] L. Rivas, C. M. Soares, A. M. Baptista, J. Simaan, R. E. Di Paolo, D. H. Murgida, P. Hildebrandt, *Biophys. J.* **2005**, *88*, 4188 – 4199.
[32] P. B. Crowley, M. Ubbink, *Acc. Chem. Res.* **2003**, *36*, 723 – 730.
[33] P. B. Crowley, M. A. Carrondo, *Proteins Struct. Funct. Bioinf.* **2004**, *55*, 603 – 612.
[34] M. Prudêncio, M. Ubbink, *J. Mol. Recognit.* **2004**, *17*, 524 – 539.
[35] B. M. Hoffman, L. M. Celis, D. A. Cull, A. D. Patel, J. L. Seifert, K. E. Wheeler, J. Y. Wang, J. Yao, I. V. Kurnikov, J. M. Nocek, *Proc. Natl. Acad. Sci. USA* **2005**, *102*, 3564 – 3569.
[36] K. E. Wheeler, J. M. Nocek, D. A. Cull, L. A. Yatsunyk, A. C. Rosenzweig, B. M. Hoffman, *J. Am. Chem. Soc.* **2007**, *129*, 3906 – 3917.
[37] P. Xiong, J. M. Nocek, A. K. K. Griffin, J. Y. Wang, B. M. Hoffman, *J. Am. Chem. Soc.* **2009**, *131*, 6938 – 6939.
[38] Z. Qing Feng, S. Imabayashi, T. Kakiuchi, K. Niki, *J. Chem. Soc. Faraday Trans.* **1997**, *93*, 1367 – 1370.
[39] A. Avila, B. W. Gregory, K. Niki, T. M. Cotton, *J. Phys. Chem. B* **2000**, *104*, 2759 – 2766.
[40] K. Fujita, N. Nakamura, H. Ohno, B. S. Leigh, K. Niki, H. B. Gray, J. H. Richards, *J. Am. Chem. Soc.* **2004**, *126*, 13954 – 13961.
[41] H. J. Yue, D. Khoshtariya, D. H. Waldeck, J. Grochol, P. Hildebrandt, D. H. Murgida, *J. Phys. Chem. B* **2006**, *110*, 19906 – 19913.
[42] D. E. Khoshtariya, T. D. Dolidze, M. Shushanyan, K. L. Davis, D. H. Waldeck, R. van Eldik, *Proc. Natl. Acad. Sci. USA* **2010**, *107*, 2757 – 2762.
[43] D. H. Murgida, P. Hildebrandt, *Acc. Chem. Res.* **2004**, *37*, 854 – 861.
[44] M. van de Kamp, F. C. Hali, N. Rosato, A. F. Agro, G. W. Canters, *Biochim. Biophys. Acta Bioenerg.* **1990**, *1019*, 283 – 292.
[45] G. J. C. van Baarle, A. M. Troianovski, T. Nishizaki, P. H. Kes, J. Aarts, *Appl. Phys. Lett.* **2003**, *82*, 1081 – 1083.

